How to cite: *Angew. Chem. Int. Ed.* **2023**, *62*, e202309402
doi.org/10.1002/anie.202309402

Liquid Crystals

Programmable and Self-Healable Liquid Crystal Elastomer Actuators Based on Halogen Bonding

Hongshuang Guo, Chen Liang, Tero-Petri Ruoko, Henning Meteling, Bo Peng, Hao Zeng, and Arri Priimagi**

Abstract: Shape-changing polymeric materials have gained significant attention in the field of bioinspired soft robotics. However, challenges remain in versatilizing the shape-morphing process to suit different tasks and environments, and in designing systems that combine reversible actuation and self-healing ability. Here, we report halogen-bonded liquid crystal elastomers (LCEs) that can be arbitrarily shape-programmed and that self-heal under mild thermal or photothermal stimulation. We incorporate halogen-bond-donating diiodotetrafluorobenzene molecules as dynamic supramolecular crosslinks into the LCEs and show that these relatively weak crosslinks are pertinent for their mechanical programming and self-healing. Utilizing the halogen-bonded LCEs, we demonstrate proof-of-concept soft robotic motions such as crawling and rolling with programmed velocities. Our results showcase halogen bonding as a promising, yet unexplored tool for the preparation of smart supramolecular constructs for the development of advanced soft actuators.

Introduction

During the past decade, polymeric materials that reversibly change shape or locomote in response to external stimuli have gained significant attention as a platform for bioinspired soft robotics.[1–5] Wireless control over material motions induced by, e.g., light[6–8] or magnetic fields[9–11] enables the miniaturization of robotic constructs, which in combination with the synthetic versatility and compliance of polymeric materials have yielded demonstrations on responsive-material-based robots that navigate in complex environments, self-adapt, and make simple decisions autonomously.[9,12] Two key features for boosting stimuli-responsive polymers in constructing advanced shape-changing soft material systems are versatile programming over material motions to adjust the specific form of deformation for the needs of different tasks and environments, and the ability to self-heal upon damage. Novel material designs able to meet these requirements under mild stimulation are in continuous demand.

In terms of obtaining programmable shape changes, liquid crystal elastomers (LCEs) are particularly promising due to facile control over the alignment of the LC mesogens during polymerization and large, anisotropic, and reversible stimuli-induced strains within the loosely crosslinked network.[13–16] As a result, advanced functionalities such as biomimetic shape-morphing, cilia-like fluidic pumping, and butterfly wing-like oscillation, have been recently demonstrated.[17–19] Self-healing LCE formulations have also been reported.[16,20–24] This characteristic requires the incorporation of dynamic bonds into LCE design, which can be obtained using, e.g., hydrogen bonds, disulfide bonds, ester bonds, and others.[20,21,23,25–29] However, a common problem with the examples demonstrated is the relatively low exchange rate of the dynamic bonds used, which leads to high stability at ambient conditions and compromises the dynamic behavior. Consequently, high operation temperatures are often required to facilitate bond exchange. There is a need to incorporate weak supramolecular bonds into LCEs, to facilitate the programmability in shape-morphing and self-healing capacity.

Looking at the toolbox of supramolecular interactions, halogen bonding (XB) stands out due to its several attractive features in the context of dynamic functional materials design.[30–32] It is a relatively weak, yet highly directional interaction between a positively charged region on a halogen atom attached to an electron-withdrawing group and a Lewis base.[33,34] XB has been extensively used in supramolecular crystal engineering and molecular recognition studies,[35–37] and its use has recently expanded towards polymer sciences and materials engineering.[38] To mention but a few potential prospects, the hydrophobic nature of XB enables the fabrication of passivated, moisture-stable perovskite solar cells,[39,40] and the large size of the bond-donating halogen atoms promote persistently

[*] Dr. H. Guo, Dr. T.-P. Ruoko, Dr. H. Meteling, Dr. H. Zeng, Prof. A. Priimagi
Faculty of Engineering and Natural Sciences, Tampere University
P.O. Box 541, 33101 Tampere (Finland)
E-mail: hongshuang.guo@tuni.fi
arri.priimagi@tuni.fi
Dr. C. Liang, Dr. B. Peng
Department of Applied Physics, Aalto University
P.O. Box 15100, 02150 Espoo (Finland)

phosphorescence emission in all-organic materials.[41–43] In the context of polymers, demonstrations on halogen-bonded supramolecular networks with intrinsic self-healing ability[44] and thermoresponsive shape memory behavior triggered by body temperature[45] prompted us to hypothesize that when incorporated as dynamic crosslinks into LCEs, XB could provide a new supramolecular tool for the design of programmable, self-healing responsive-material-based actuators.

Herein, we verify the above hypothesis and present halogen-bonded, shape-programmable LCEs that can self-heal under mild temperature stimulation. The material design combines weak XB crosslinks and stronger (yet still dynamic) disulfide-containing crosslinks in an anisotropic LCE. The weak and strong crosslinks together yield the desired mechanical properties to promote self-healing and mechanical programming through reversibly breaking the XB crosslinks, and reversible actuation in response to temperature and light stimuli. As proof-of-concept robotic demonstrations, we devise shape-programmed walking and rolling robots from the XB-based LCEs.

Results and Discussion

The design concept of the XB-based LCE actuator is illustrated in Figure 1. We use the Aza-Michael addition reaction between RM82, a standard diacrylate mesogen, and two different amines, to prepare chain-extended, main-chain LCEs.[46,47] Therein, cystamine (**1**) serves as a dynamic

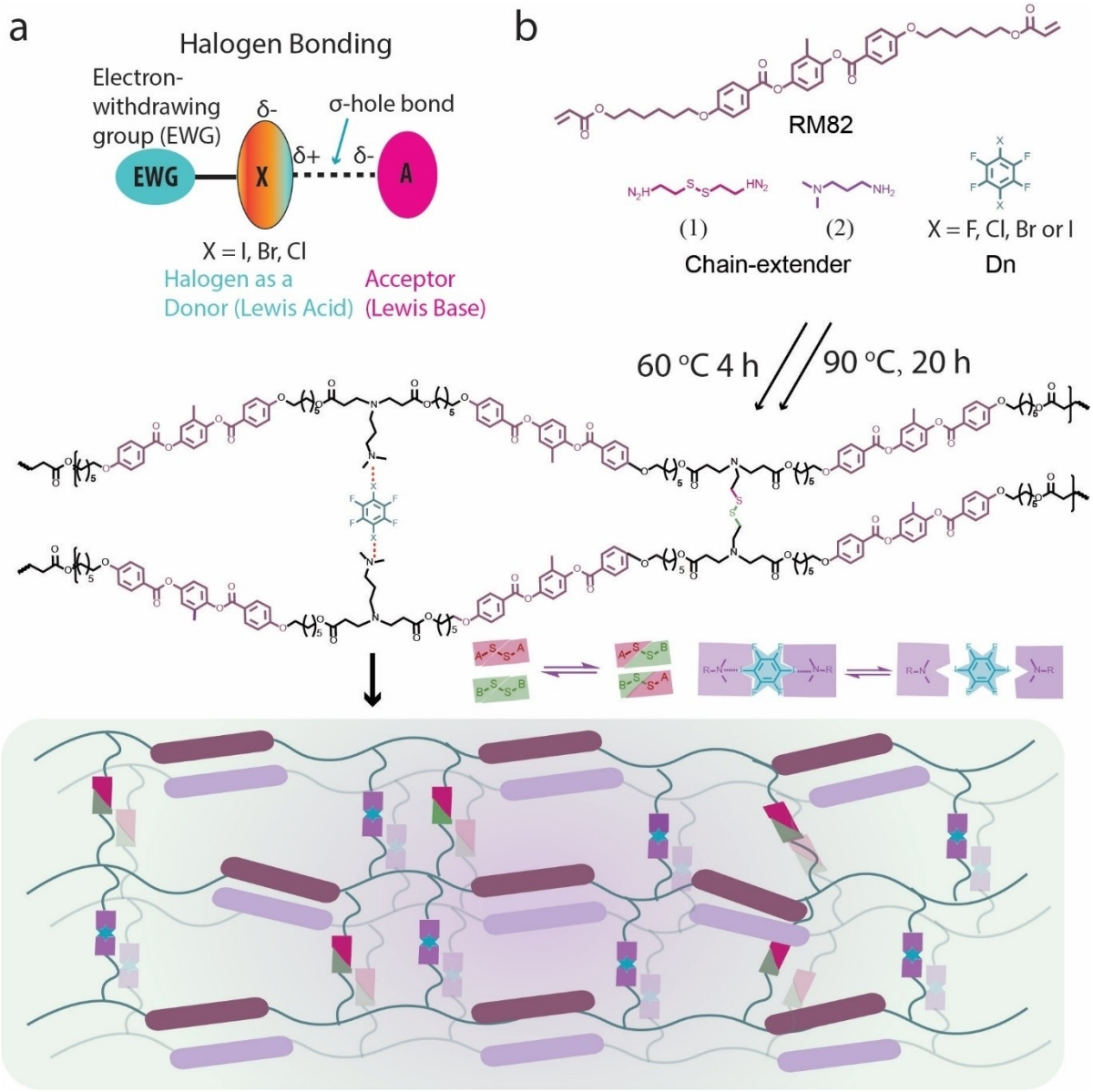

Figure 1. The Material Design Concept. (a) Schematic representation of the halogen bond. (b) The chemical composition and preparation process of the halogen-bond-based LCE and schematic representation of the corresponding supramolecular network.

covalent crosslinker which, due to its strong absorption in the near-UV region, also allows for photothermal activation of the LCE.[48] Whereas the disulfide exchange reaction can also promote self-healing, the process requires relatively high temperatures, and below 80 °C, **1** behaves essentially as permanent crosslinks.[26,49,50]

Halogen bonding takes place between the electron-deficient area (the σ-hole) of a polarizable halogen atom (typically I, Br) and a Lewis base (Figure 1a).[33,34] Herein, we used 1,4-diiodotetrafluorobenzene (denoted as $D_{1,4I}$), a common difunctional XB donor, and complexed with N,N-dimethylamino-propylamine (**2**) that was used as an XB-accepting chain extender, to yield dynamic supramolecular crosslinks within the stimuli-responsive LCE network (Figure 1b). According to density functional theory (DFT) calculations (PEBPEB/6-311++G (d,p) level of theory for all atoms except iodine, for which 6-311G (d,p) was used; see Supporting Information for further details), the stabilization energy between $D_{1,4I}$ and N,N-dimethylamino acceptor is *ca.* −5.5 kcal mol^{-1}, which is in the same range as for more commonly used pyridine acceptors.[51,52] Herein, N,N-dimethylaminobutane (**3**) was used as a substitute for **2** to exclude the potential influence of non-polymerized -NH_2 groups on the XB formation. Based on our previous work[45] we anticipate that the XB-based dynamic crosslinks enable tuning of the material stiffness, which is crucial for self-healing and programmability under mild conditions.[53]

Unless otherwise stated, the Aza-Michael addition reaction was conducted with a mixture containing RM82, **1**, **2**, and $D_{1,4I}$ in a ratio of 10:3:4:2, i.e., a fixed 2:1 ratio between the N,N-dimethylamino XB acceptors and perfluorinated XB donors, as well as acrylate and amine groups taking part in the chain extension reaction, was used. The resulting elastomer network is denoted as LCE-$D_{1,4I}$. To verify the role of XB, $D_{1,4I}$ was replaced with several perfluorinated analogues (Figure S1) to study the mechanical properties of corresponding elastomer networks with varying interaction strength (Figures S2a–e) with the N,N-dimethylamino acceptor: **3**·$D_{1,4I}$ (−5.5 kcal mol^{-1}) > **3**·$D_{1,4Br}$ (−2.9 kcal mol^{-1}) > **3**·$D_{1,4Cl}$ (−0.4 kcal mol^{-1}) ≫ **3**·$D_{1,4F}$ (not detected).[54] Substitution with electronegative fluorine atoms plays an important role in strengthening the XB-donating ability of $D_{1,4I}$ (as well as $D_{1,4Br}$; due to the low polarizability of chlorine atoms, the XB strength for $D_{1,4Cl}$ is negligible), yielding a more positive potential of the σ-holes as compared to non-perfluorinated analogues.[51] $D_{1,4F}$ acts as a nonbonding reference molecule, as F can act as an XB donor only in connection with particularly strong electron-withdrawing groups.[55]

In addition to DFT calculations, the XB formation between dimethylamino and the XB donors was studied with Raman spectroscopy on both the LCEs (e.g. LCE-$D_{1,4I}$) and non-polymerized 2:1 mixtures of the XB donors with N,N-dimethylaminobutane (**3**) (e.g. **3**·$D_{1,4I}$). The signal characteristic of uncomplexed C–X bond is located at 100–400 cm^{-1} and red shifts upon XB formation.[53,56] As shown in Figure 2a and Figure S3, both **3**·$D_{1,4I}$ and LCE-$D_{1,4I}$ show clear red shifts compared to plain $D_{1,4I}$, implying a weaker C–I bond force constant due to the n→σ* nature of the I···N interaction.[57] The red shift is larger in LCE-$D_{1,4I}$ compared to **3**·$D_{1,4I}$, implying that other physical interactions occurring in the polymer network that are not present in the small-molecule complex may strengthen the XB interaction. Conversely, complexes bearing $D_{1,4Br}$, $D_{1,4Cl}$, or $D_{1,4F}$ (Figures S4–S6) exhibited no C–X frequency shifts compared to the corresponding uncomplexed donors, indicating no XB formation.

We next explored the thermodynamic and mechanical properties of the LCEs. The glass transition temperature (T_g) of the elastomer networks containing different donors ranges from −8 to 1 °C, as measured using differential scanning calorimetry (DSC; Figure 2b, Figures S7a–d, Table 1). LCE-$D_{1,4I}$ exhibited the highest T_g of 1 °C, which could be expected due to the presence of the I···N bonds. In contrast, LCE-$D_{1,4Br}$, LCE-$D_{1,4Cl}$, and LCE-$D_{1,4F}$ all had T_g values around −8 °C, indicating higher chain flexibility. The mechanical properties were probed via uniaxial stretching of corresponding LCE strips (16×2×0.5 mm^3), as exemplified in Figure 2c. LCE-$D_{1,4I}$ has an elastic modulus of 3.8 MPa, tensile strength of 2.6 MPa, and fracture strain of 251 %. LCE-$D_{1,4Br}$, LCE-$D_{1,4Cl}$, and LCE-$D_{1,4F}$ were softer at room temperature and had low tensile strengths, while the fracture strains remained above 200 % (Table 1), indicating that the presence of XB led to an increase in both elastic modulus and tensile strength. We also compared the mechanical properties at room temperature and 50 °C. Figures S8a–d indicate that all LCEs became soft upon heating, leading to a decrease in elastic modulus, tensile strength, and fracture strain. However, the temperature-induced decrease in the elastic modulus (from 3.4 MPa to 0.7 MPa) is much more pronounced in LCE-$D_{1,4I}$ compared to the other LCEs, implying that at this temperature, a large fraction of halogen bonds are broken.

We also conducted dynamic mechanical analysis (DMA) for the LCEs (16×2×0.5 mm^3) to characterize their dynamic viscoelastic properties (Figure 2d). The thermogram shows that the storage modulus (E′) inflection points and loss tangent (tan δ) peak maximum occur at around 35 °C for LCE-$D_{1,4I}$ and range from 8–13 °C for the other LCEs studied. This difference again points towards the role of XB in altering the thermomechanical properties of the networks. The α-relaxation transition of the LCEs without XB occurred at lower temperatures than for LCE-$D_{1,4I}$, and a decrease in E′ observed in the rubbery plateau region can be attributed to weak physical crosslinking that does not involve halogen bonds.[58] As the temperature increased, the

Table 1: Mechanical properties and glass transition temperature (T_g) of XB elastomers. The elastic moduli (E_Y), tensile strengths (σ_{max}), and fracture strains (ε_{max}) have been obtained by averaging over three different samples.

Code	E_Y (MPa)	σ_{max} (MPa)	ε_{max} (%)	T_g (°C)
LCE-$D_{1,4I}$	3 ± 0.2	2.6 ± 0.5	251 ± 17	1
LCE-$D_{1,4Br}$	1.4 ± 0.2	1.8 ± 0.3	228 ± 16	−7
LCE-$D_{1,4Cl}$	0.8 ± 0.1	1.3 ± 0.4	217 ± 16	−7
LCE-$D_{1,4F}$	1.8 ± 0.3	1.8 ± 0.3	228 ± 22	−8

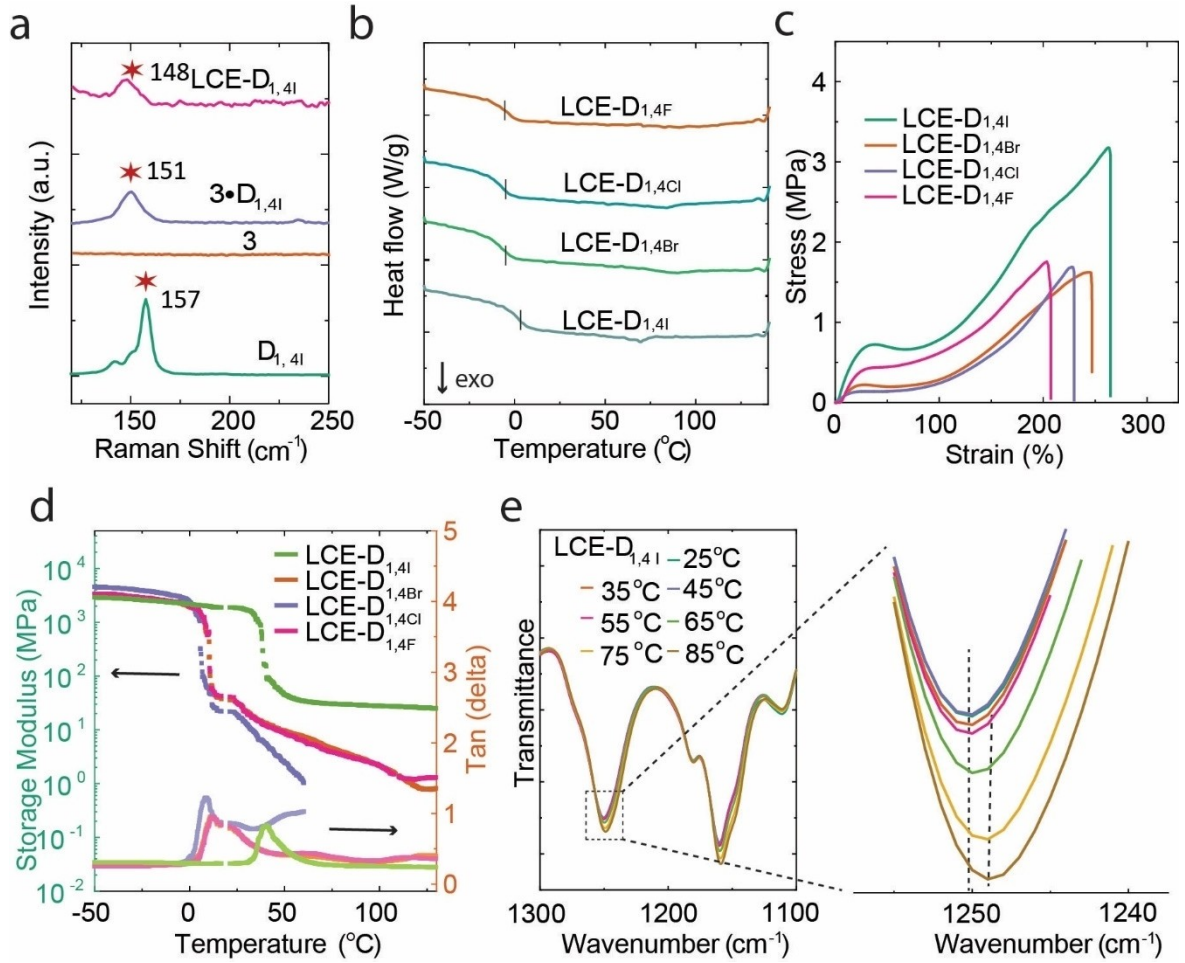

Figure 2. Materials Characterization. (a) Raman spectrum of $D_{1,4I}$, **3**, **3**·$D_{1,4I}$, and LCE-$D_{1,4I}$, indicating a red shift of the C–I stretching band due to XB formation. (b) DSC curves, (c) stress-strain curves, and (d) DMA curves of storage modulus (E′) and loss tangent (tan δ) as a function of temperature, of the LCEs studied. The DSC data is taken from the second cooling cycle at a heating/cooling rate of 10 °C/min. The DMA curves for LCE-$D_{1,4Cl}$ could only be measured up to 60 °C above which the samples became overly soft. (e) FTIR spectra of LCE-$D_{1,4I}$ upon heating from 25 to 85 °C (interval: 10 °C).

materials entered the viscoelastic flow region, where an increase in tan δ and a decrease in E′ indicated the onset of the melting transition of the liquid crystalline region. We note that based on the Raman analysis as well as the DSC data, only LCE-$D_{1,4I}$ forms a halogen-bonded network. Hence the minor differences observed in the mechanical properties of the other three samples are likely to arise from differences in nonspecific intermolecular interactions and molecular packing, not from XB.

We verified that XB can be opened under moderate heating using temperature-dependent fourier transform infrared (FTIR) spectroscopy (Figure 2e, Figures S9a–d, and Figures S10a–d). The C–N stretch of the N,N-dimethylamino group is located in the absorption range of 1100–1300 cm^{-1} (Figures S9a–d).[59] The stretching vibration peaks at 1161 cm^{-1} and 1251 cm^{-1} remained unaffected up to 45 °C, after which the peaks shifted to lower wavenumbers, to 1159 cm^{-1} and 1248 cm^{-1}, respectively (Figure 2e).[60] The peak shift was only observed for LCE-$D_{1,4I}$ and is absent for other donors (Figures S10a–d). This attests that at temperatures below ca. 55 °C, the majority of XB crosslinks retain, forming a supramolecular network that ensures the material's mechanical stability. Above this temperature, the XBs are gradually broken, which, as will be shown, allows for self-healing and shape programming that is fixed upon cooling due to the thermo-reversibility of the XBs.

Based on the above results, we conclude that all two-component donor-acceptor polymers, except LCE-$D_{1,4I}$, are mechanically weak and possess rather similar tensile strength profiles, making them unsuitable for actuator applications. The I···N XB increases the mechanical strength of the elastomer networks, and LCE-$D_{1,4I}$ combines a relatively high modulus and fracture strain. Therefore, only LCE-$D_{1,4I}$ is used in further experiments on reversible actuation and self-healing.

The LCE-$D_{1,4I}$ is in an isotropic polydomain state (Figure 3a) after photopolymerization (see Supporting Information for polymerization details), as confirmed by lack of contrast during sample rotation in polarized optical micrographs (Figure S12). Upon uniaxial stretching (100 %), the

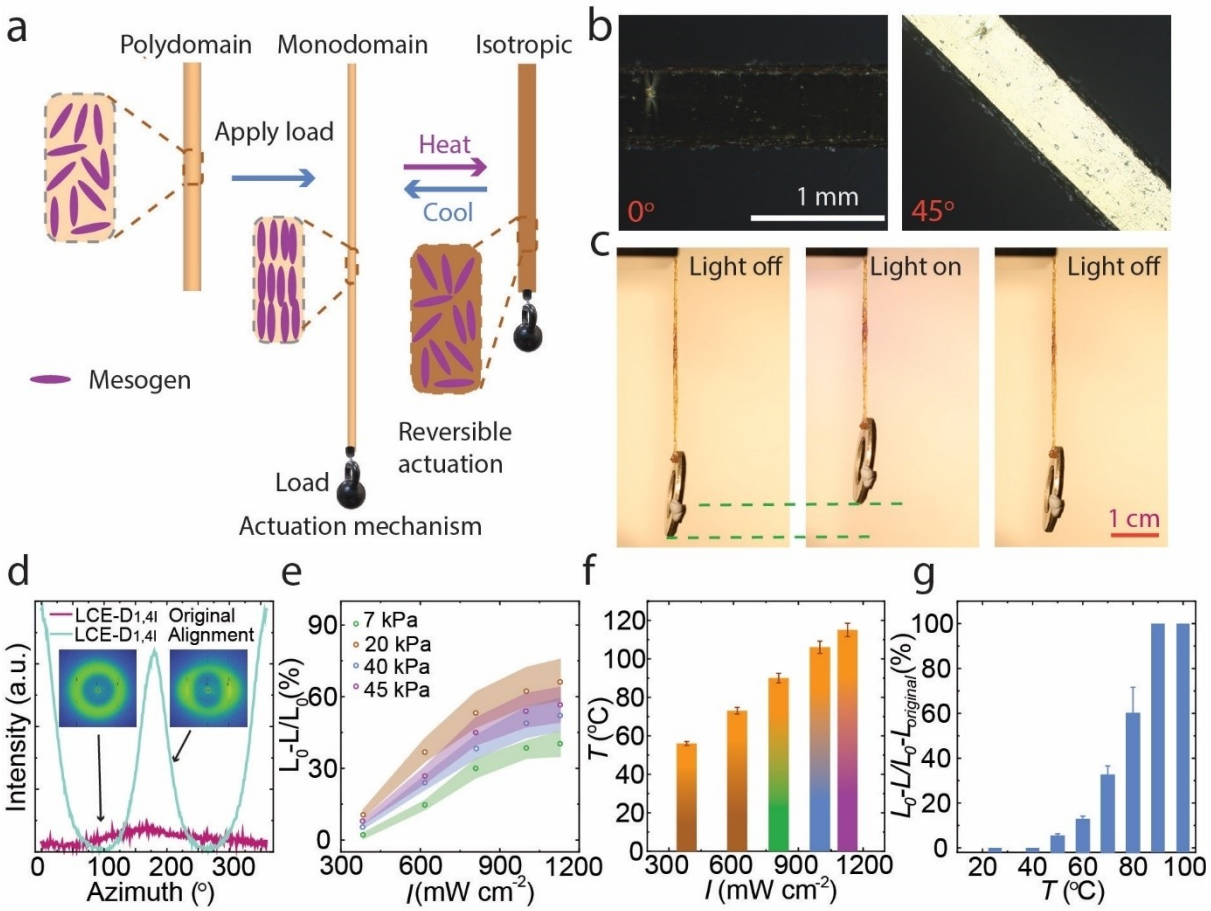

Figure 3. Thermal and photothermal actuation of LCE-$D_{1,4I}$. (a) Schematic illustration of the actuation of LCE-$D_{1,4I}$. The film is initially in an isotropic, polydomain state, but gets uniaxially aligned upon stretching. Upon heating, the uniaxial alignment is gradually lost, causing reversible contraction along the stretching direction upon heating. (b) Polarized optical micrographs of the stretched LCE-$D_{1,4I}$ at 0° and 45° angles between the molecular director and the polarizer/analyzer, attesting uniaxial molecular alignment. (c) Photographs of photothermal actuation of the LCE-$D_{1,4I}$ under mechanical load (365 nm, 1000 mW cm^{-2}). (d) 1D azimuthal scan profiles for the LCE-$D_{1,4I}$ strip. Insets: 2D WAXS patterns of the LCE-$D_{1,4I}$ strip before and after stretching (100%). (e) Photoinduced contraction of LCE-$D_{1,4I}$ under different loads and using different light intensities. (f) Light-induced temperature elevation of the LCE-$D_{1,4I}$ film. Light: 365 nm. (g) Contraction under uniform heating. In (e) and (g), L_0 stands for the initial length (after stretching) and L is the contracted length under light irradiation (Figure S11). $L_{original}$ is the initial length before stretching.

film becomes strongly anisotropic as the LC mesogens align along the stretching direction (see Figure 3b for POM images). When the stretched monodomain film is heated, the molecular order is lost, resulting in a large uniaxial contraction (60% upon heating to 80 °C). Upon cooling, the molecular order is retained, and the film restores its original length. Since the disulfide-containing crosslinks absorb at 365 nm, the contraction can be reversibly controlled with light via photothermal heating, as shown in Figure 3c and Supplementary Movie 1.

The anisotropic molecular orientation of LCE-$D_{1,4I}$ was studied with wide-angle X-ray scattering (WAXS; Figure 3d). The ring-shaped isotropic WAXS pattern and featureless scattering curve before stretching confirm the random molecular orientation. After stretching, the monodomain molecular alignment results in strong scattering peaks perpendicular to the stretching direction, suggesting a high degree of orientational ordering during stretching.[24,61] The order parameter of the stretched LCE-$D_{1,4I}$ was deduced using the Hermans–Stein orientation distribution function,[62] yielding a value of 0.66 upon 100% stretching. The WAXS patterns at elevated temperatures confirm the gradual loss of molecular alignment (rather than distinct, well-defined order-to-disorder phase transition), yielding order parameters of 0.6, 0.54, and 0.43 at 50, 75, and 100 °C, respectively (Figures S13a–c). The corresponding scattering peak was found at 1.4 Å^{-1}, indicating an intermolecular distance of neighbouring mesogens of ca. 4.5 Å (Figure S13d). The aligned LCE-$D_{1,4I}$ film also exhibits two spots at small-angle regions (Figure S13e) perpendicular to the arcs in the wide-angle region, suggesting the formation of smectic layers upon stretching with a layer thickness of ca. 5 nm (Figure S13d).[63]

The actuation performance of the stretched LCE-$D_{1,4I}$ was further investigated by applying a load on the film and measuring its contraction as a function of light intensity and temperature. The photocontraction was driven by photothermal heating (Figure S14) and was hence strongly light-

intensity-dependent (Figure 3e): at 1100 mW cm^{-1}, the surface temperature reached 108 °C (Figure 3f) and the obtained contraction was 65 %, 55 %, 50 %, and 35 % when applying a load of 7, 20, 40, and 45 kPa, respectively. The photocontraction is reversible although fatigue could be observed after tens of irradiation cycles due to the relatively high light intensity used (Figure S15). Upon heating with no external load, LCE-$D_{1,4I}$ yields 100 % contraction at 90 °C due to the reduced molecular alignment order (Figure 3g).

We next investigated the self-healing properties of LCE-$D_{1,4I}$. The healing indeed took place under moderate heating and without applying external pressure; it was enough that the cut parts were placed in contact under appropriate conditions (typically 80 °C for 5 min). To understand the role of XB in self-healing, we conducted several control experiments, varying the ratio between the disulfide and XB crosslinks (Figures S16a–d). For an LCE containing only the disulfide crosslinks (RM82:**1**:**2**:$D_{1,4I}$ ratio 10:5:0:0), the healing (80 °C for 5 min without applying external pressure) was practically non-existent due to a high density of covalent crosslinks and the absence of the dynamic supramolecular bonds. On the other hand, if the LCE contained XB crosslinks (RM82:**1**:**2**:$D_{1,4I}$ ratio 10:0:10:5) only, the sample was mechanically weak and too soft to be handled and manipulated. Hence, a combination of both types of crosslinks was needed to necessitate self-healing. By doubling the number of XB crosslinks (RM82:**1**:**2**:$D_{1,4I}$ ratio 10:1:8:4), the healing was even more efficient than for the LCE-$D_{1,4I}$ (Figure S16c) due to which this ratio was chosen for further characterization.

The self-healing under mild stimulation is illustrated in Figure 4a, showing that two cut pieces of an LCE strip with XB crosslinks could be connected by keeping them in contact for 5 min at 80 °C. The healed sample can be stretched up to 300 % without rupture, and it maintains its actuation performance. Under 40 kPa loading, the healed sample reversibly contracts by 40 % under 365 nm, 1000 mW cm^{-2} irradiation (Figure 4b, Supplementary Movie 2). Figures 4c and d depict the representative stress-strain curves and healing efficiency for samples healed at different temperatures. Increasing the temperature (while keeping the healing time fixed at 5 min) enhances the fracture strain of the healed sample, the healing efficiency being 22 % at 40 °C and 60 % at 110 °C. The difference in healing efficiency at 110 °C compared to 80 °C was minute, possibly because most halogen bonds were already broken at 80 °C. As shown in Figures 4e and f, at 80 °C 60 % a healing efficiency is reached within 5 min and was not further improved by prolonged healing time.

The self-healing can also be induced with light via photothermal heating (Figure 4g and Figure S17, Supplementary Movie 3). After cutting the LCE and bringing the fractured surfaces into contact, we exposed them to 365 nm irradiation (600 mW cm^{-2}) for 5 min, yielding a temperature increase close to 80 °C (Figure 3f). The healing efficiency was close to 50 %, and the sample could be stretched up to 200 % without breaking. We also speculated that the hydrophobicity of the halogen bond could yield self-healing induced by hot water, which prompted us to put two cut pieces of LCE in contact in an 80 °C hot water bath for 5 min. The underwater self-healing was moderate, but even in this case, the sample could be stretched up to 130 % without breaking. The reduced healing efficiency in hot water is ascribed to the decrease of physical contact between two cut surfaces because of the presence of water between them.

Our findings indicate that XB plays a crucial role in material healing for two reasons: (1) it can modulate the mechanical properties of the material (Figures S16a and S16b); (2) it is a dynamic bond that breaks upon moderate heating. The hypothesized healing mechanism of LCE-$D_{1,4I}$ is shown in Figure S18, where the dynamic bonds open as the temperature rises and reassemble as the temperature decreases. The LCE-$D_{1,4I}$ exhibits stable and reversible actuation performance after cutting and healing (Figure S19).

Figure 2e indicates that the halogen bonds gradually break at ca. 55 °C. Hence, we postulate that above this temperature, LCE-$D_{1,4I}$ can be programmed to adapt different shapes which can then be reversibly actuated. This is demonstrated in Figure 5a, which presents six differently shaped LCEs obtained by mechanically deforming them at 55 °C and subsequently cooling them to room temperature. After cooling, the samples were left to equilibrate for 3 days under ambient conditions, after which they were indeed reversibly transformed between the programmed shape and the initial shape through heat stimulus (Figure 5a), i.e., they underwent a two-way shape-memory effect.[58] Due to the weak supramolecular bonds used, the shape programming does not necessitate high temperatures, rendering it rather unique among the shape-programmable LCEs.[21] We note that the long equilibration time is critical for the reversible actuation, presumably to allow the dynamic halogen bonds to undergo multiple reorganizations. If the LCE-$D_{1,4I}$ is shape-programmed and actuated without equilibration, it exhibits an irreversible, one-way shape memory effect (Figure S20).

The prolonged equilibration period for reversible shape change can be attributed to factors such as the need to eliminate initial non-uniformities or stresses, as observed in some LCEs.[64] When LCE-$D_{1,4I}$ is subjected to stretching at an elevated temperature, the dynamic halogen bonds are disrupted, creating internal stresses within the material upon cooling. These initial stresses gradually equilibrate, leading to slow contraction of the LCE strip over several days (Figure S21a). XB disruption and reformation are evident in FTIR data (Figure S21b). Immediately after stretching and cooling, the N,N-dimethylamino group's stretching vibration peak is at 1249 cm^{-1}, indicating no halogen bonding (cf. Figure 2e). Over several days, this peak shifts to 1251 cm^{-1}, signifying gradual XB reformation and strengthening of the XB crosslinks (Figure S21c). Notably, without halogen bonds (LCE-$D_{1,4Br}$, LCE-$D_{1,4Cl}$, LCE-$D_{1,4F}$), no reversible actuation is achieved even after extended equilibration. Mechanical testing and Raman analysis of samples equilibrated for different times reveal that LCE-$D_{1,4I}$ has a fracture strain of only 48 % immediately after stretching and cooling due to the absence of dynamic XB crosslinks and

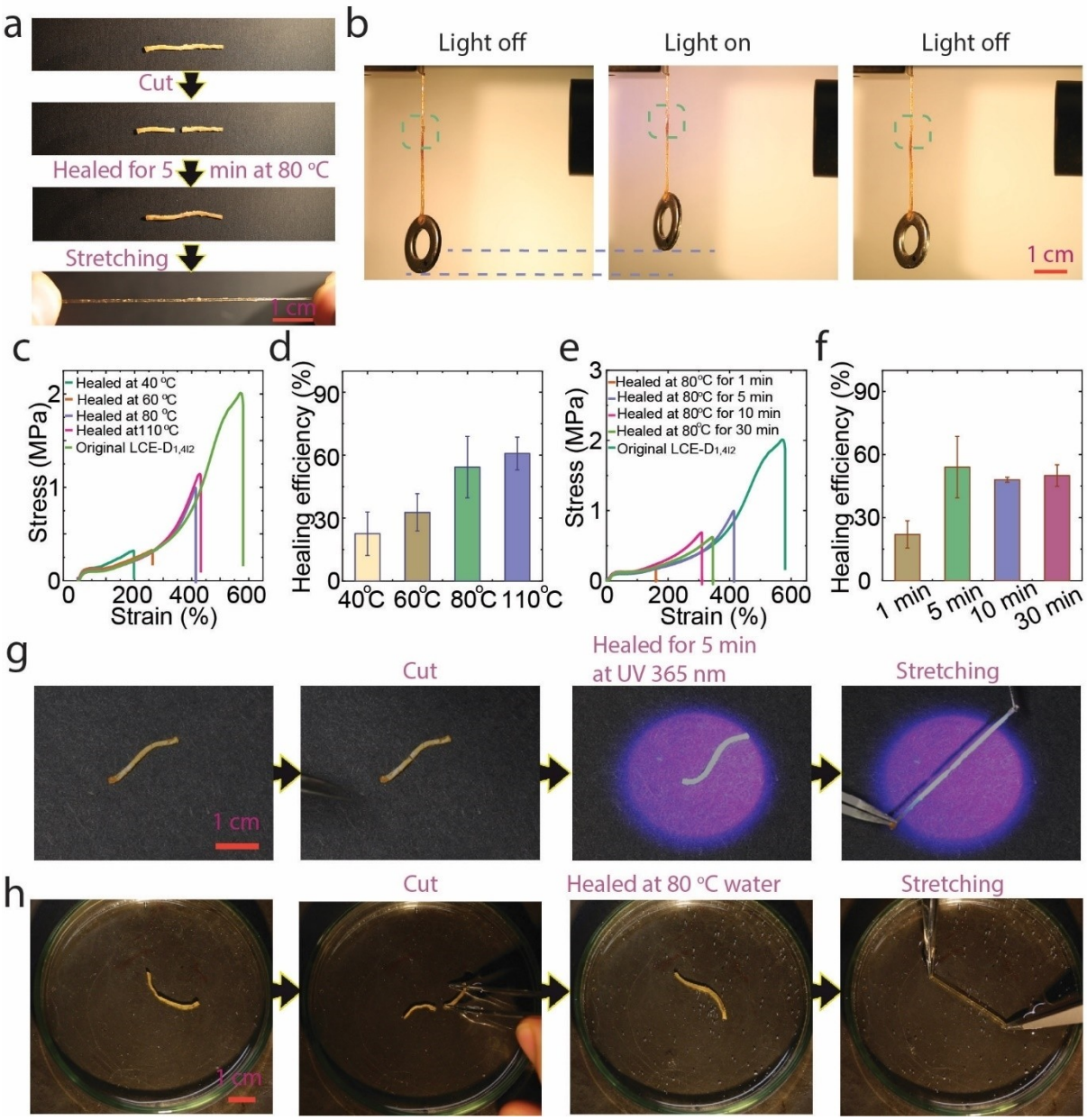

Figure 4. Self-healing of the halogen-bond-crosslinked LCEs. (a) Photographs of the self-healing process of two LCE segments bearing XB crosslinks. After self-healing, the LCE could be stretched >300% without rupture. Sample dimensions: 20×1.0×0.5 mm^3. (b) Photographs of photothermal actuation after self-healing (365 nm, 1000 $mW\,cm^{-2}$). Sample dimensions: 40×1.0×0.5 mm^3. (c) Tensile stress-strain curves of the original LCE strip and the strip healed at different temperatures and (d) corresponding healing efficiencies. (e) Tensile stress-strain curves of the original LCE strip and the strips healed for different times at 80 °C, and (f) corresponding healing efficiencies. (g) Photograph of the light-induced self-healing process (365 nm, 600 $mW\,cm^{-2}$). After healing, the LCE strip could be stretched 200% without rupture. Sample dimensions: 20×1.0×0.5 mm^3. (h) Photograph of the self-healing taking place in a hot bath (80 °C water). After healing, the LCE strip could be stretched 130% without rupture. Sample dimensions: 20×1.0×0.5 mm^3. All the error bars in the Figure indicate the standard deviation for n=3 measurements.

the presence of only covalent disulfide crosslinks. Over 3 days, the reformation of XB crosslinks increases the fracture strain to >100%. In contrast, LCE-$D_{1,4Cl}$ control (lacking XB interactions) does not exhibit the XB-induced shift in the stretching vibration peak of the N,N-dimethylamino group and experiences a decreasing Young's modulus over time (Figure S22b). The role of XB is further supported by Raman analysis (Figure S22c), showing that with increasing equilibration time, XBs gradually form and the Raman peak red shifts. These data confirm the essential role that XB plays in the reorganization and equilibration process needed for reversible actuation.

The shape-programmable, reversible (photo)actuation can be used for demonstrating different kinds of soft robotic motions. Figure 5A iii presents a twisted spring of LCE-$D_{1,4I}$ which can act as an artificial filament to provide muscle-like

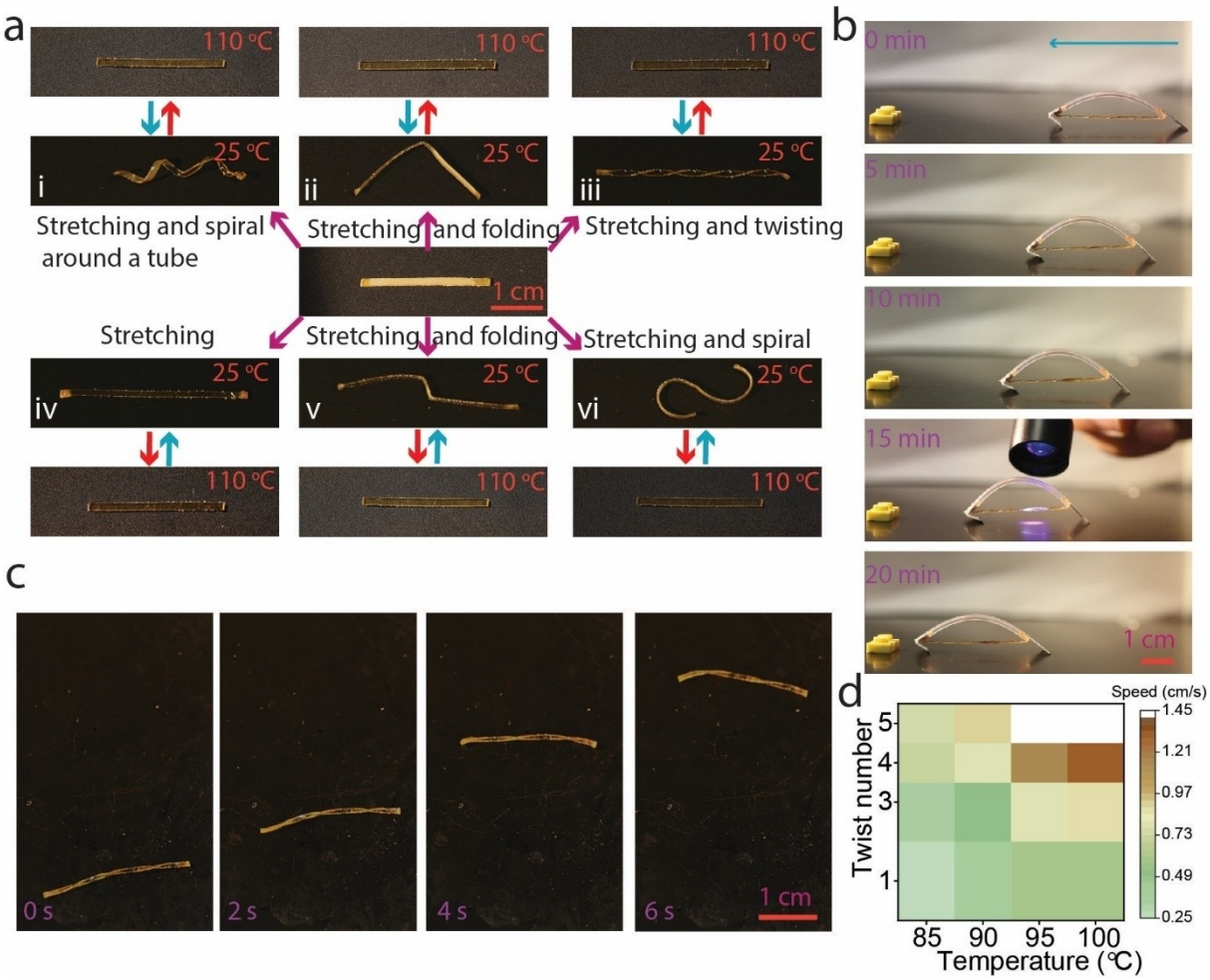

Figure 5. Programmable halogen-bonded LCE actuators. (a) Photographs of shape-programmed LCE-$D_{1,4I}$ strips. The programming was done at 55 °C, after which the shapes could be reversibly actuated upon temperature stimulus. (b) LCE-$D_{1,4I}$ walker under cyclic UV illumination (800 mW cm^{-2}). Actuator dimension: 20×2 ×0.4 mm^3. (c) Photographs of LCE-$D_{1,4I}$ undergoing rolling locomotion on a 95 °C hot plate. Actuator dimension: 24×1×0.4 mm^3. (d) Color map summarizing the speed upon different temperatures and twist numbers.

contraction. Herein, we integrate this filament between a bent plastic to create a light-controlled walking robot with reversible body bending. As illustrated in Figure 5b and Supplementary Movie 4, the structure moves on a flat glass substrate over one body length (4 cm) in 20 min under cyclic light irradiation (Figure S23), driven by the asymmetry of the frictional forces in the forward and backward directions (Figure S24). The twisted LCE-$D_{1,4I}$ also exhibits autonomous rolling motion on a hot plate set at 95 °C (Figure 5c and Supplementary Movie 5). The motion is driven by contraction of the twisted LCE strip that is in contact with the hot plate, causing rotation, after which the contracted parts cool down and expand while the rest parts of the LCE are exposed to heat, leading to self-propelled, zero-energy-mode deformation fueled by the thermal gradient.[65] By controlling the degree of twisting during the shape programming, the rolling speed can be tuned (Figure 5d): The larger the twisting angle, the faster the rolling speed. At a fixed twisting angle, the rolling speed gradually increases with the hot plate temperature. The self-sustained rolling can be retained in a self-healed LCE (Figure S25 and Supplementary Movie 6), indicating the utility of XB not only in shape programming at low temperatures and reversible actuation for soft robotic motions but also in retaining these motions after repair from damage. These findings point to an important materials design direction for dynamic soft actuators, in which halogen bonding will have lots to offer.

Conclusion

We present arbitrarily shape-programmable and self-healing liquid crystal elastomers (LCEs) driven by halogen bonding, a non-covalent interaction that can be considered as the weaker and more directional counterpart of (single) hydrogen bonding.[66] Due to weak and dynamic I···N crosslinks incorporated into the LCE, mild temperature stimulation suffices to break the bonds, which is critical for facile shape-programming and self-healing. We employ 1,4-diiodotetrafluorobenzene as the optimal bifunctional halogen-bond

donor and show that when it is replaced with weaker halogen-bond donors (e.g. 1,4-dibromotetrafluorobenzene) or non-bonding perfluorobenzenes (hexafluorobenzene), the shape-programming and self-healing properties are lost. We demonstrate the proof-of-concept robotic motions such as photothermally driven locomotion under pulsed irradiation and self-sustained rolling driven by thermal gradient, taking place both before and after healing. Our results highlight the promise of halogen bonding as a design tool for dynamically programmable soft actuators.

Acknowledgements

This work is supported by the European Research Council (Consolidator Grant project MULTIMODAL, agreement no 101045223 for A.P.; Starting Grant project ONLINE, agreement no. 101076207 for H.Z.). We acknowledge financial support from the Academy of Finland, provided through Academy Postdoctoral Researcher projects (No. 347201 for H.G. and No. 340103 for T.P.R.) and Academy Research Fellowship project (No. 321443 and 328942) for B.P. This work is conducted as part of the Academy of Finland Center of Excellence "Life-Inspired Hybrid Materials Research" (LIBER, No. 346107) and the Academy of Finland Flagship Programme on Photonics Research and Innovation (PREIN, No. 320165). T.P.R acknowledges the European Union's Horizon 2020 research and innovation programme under the Marie Skłodowska-Curie grant agreement No. 101022777. This work made use of Tampere Microscopy Center facilities at Tampere University and OtaNano-Nanomicroscopy Center at Aalto University (Aalto-NMC), and computing time from CSC-IT center for science. We thank Dr. Ville Liljeström for the help with SAXS Characterization.

Conflict of Interest

There are no conflicts to declare.

Data Availability Statement

The data that support the findings of this study are available from the corresponding author upon reasonable request.

Keywords: Halogen Bond · Liquid Crystal Elastomer · Programmable · Self-Healing · Soft Actuator

[1] O. Vybornyi, S.-X. Liu, R. Häner, *Angew. Chem. Int. Ed.* **2021**, *60*, 25872.
[2] X. Wang, H. Sun, Y.-K. Kim, D. B. Wright, M. Tsuei, N. C. Gianneschi, N. L. Abbott, *Adv. Mater.* **2022**, *34*, 2106535.
[3] L. Montero de Espinosa, W. Meesorn, D. Moatsou, C. Weder, *Chem. Rev.* **2017**, *117*, 12851.
[4] J. Michalska-Walkowiak, B. Förster, S. Hauschild, S. Förster, *Adv. Mater.* **2022**, *34*, 2108833.
[5] H. Sun, C. P. Kabb, M. B. Sims, B. S. Sumerlin, *Prog. Polym. Sci.* **2019**, *89*, 61.
[6] H. Shahsavan, A. Aghakhani, H. Zeng, Y. Guo, Z. S. Davidson, A. Priimagi, M. Sitti, *Proc. Natl. Acad. Sci. USA* **2020**, *117*, 5125.
[7] B. Zuo, M. Wang, B.-P. Lin, H. Yang, *Nat. Commun.* **2019**, *10*, 4539.
[8] A. H. Gelebart, D. Jan Mulder, M. Varga, A. Konya, G. Vantomme, E. W. Meijer, R. L. B. Selinger, D. J. Broer, *Nature* **2017**, *546*, 632.
[9] W. Hu, G. Z. Lum, M. Mastrangeli, M. Sitti, *Nature* **2018**, *554*, 81.
[10] Y. Dong, L. Wang, N. Xia, Z. Yang, C. Zhang, C. Pan, D. Jin, J. Zhang, C. Majidi, L. Zhang, *Sci. Adv.* **2022**, *8*, eabn8932.
[11] Z. Ren, R. Zhang, R. H. Soon, Z. Liu, W. Hu, P. R. Onck, M. Sitti, *Sci. Adv.* **2021**, *7*, eabh2022.
[12] O. M. Wani, H. Zeng, A. Priimagi, *Nat. Commun.* **2017**, *8*, 15546.
[13] K. M. Herbert, H. E. Fowler, J. M. McCracken, K. R. Schlafmann, J. A. Koch, T. J. White, *Nat. Rev. Mater.* **2022**, *7*, 23.
[14] T. J. White, D. J. Broer, *Nat. Mater.* **2015**, *14*, 1087.
[15] F. Lancia, A. Ryabchun, N. Katsonis, *Nat. Chem. Rev.* **2019**, *3*, 536.
[16] M. O. Saed, A. Gablier, E. M. Terentjev, *Chem. Rev.* **2022**, *122*, 4927.
[17] Z. Deng, H. Zhang, A. Priimagi, H. Zeng, *Adv. Mater.* **2023**, https://doi.org/10.1002/adma.202209683.
[18] Y. Zhao, Q. Li, Z. Liu, Y. Alsaid, P. Shi, M. Khalid Jawed, X. He, *Sci. Robot.* **2023**, *8*, eadf4753.
[19] T. S. Hebner, K. Korner, C. N. Bowman, K. Bhattacharya, T. J. White, *Sci. Adv.* **2023**, *9*, eade1320.
[20] Z. Wang, H. Tian, Q. He, S. Cai, *ACS Appl. Mater. Interfaces* **2017**, *9*, 33119.
[21] Z. Pei, Y. Yang, Q. Chen, E. M. Terentjev, Y. Wei, Y. Ji, *Nat. Mater.* **2014**, *13*, 36.
[22] Z. Wang, S. Cai, *J. Mater. Chem. B* **2020**, *8*, 6610.
[23] Y. Wu, Y. Yang, X. Qian, Q. Chen, Y. Wei, Y. Ji, *Angew. Chem. Int. Ed.* **2020**, *59*, 4778.
[24] Z.-C. Jiang, Y.-Y. Xiao, L. Yin, L. Han, Y. Zhao, *Angew. Chem. Int. Ed.* **2020**, *59*, 4925.
[25] Y. Yang, E. M. Terentjev, Y. Zhang, Q. Chen, Y. Zhao, Y. Wei, Y. Ji, *Angew. Chem. Int. Ed.* **2019**, *58*, 17474.
[26] Q. He, Z. Wang, Y. Wang, Z. Song, S. Cai, *ACS Appl. Mater. Interfaces* **2020**, *12*, 35464.
[27] S. Huang, Y. Shen, H. K. Bisoyi, Y. Tao, Z. Liu, M. Wang, H. Yang, Q. Li, *J. Am. Chem. Soc.* **2021**, *143*, 12543.
[28] X. Qian, Q. Chen, Y. Yang, Y. Xu, Z. Li, Z. Wang, Y. Wu, Y. Wei, Y. Ji, *Adv. Mater.* **2018**, *30*, 1801103.
[29] L. Chen, H. K. Bisoyi, Y. Huang, S. Huang, M. Wang, H. Yang, Q. Li, *Angew. Chem. Int. Ed.* **2021**, *60*, 16394.
[30] G. Cavallo, P. Metrangolo, R. Milani, T. Pilati, A. Priimagi, G. Resnati, G. Terraneo, *Chem. Rev.* **2016**, *116*, 2478.
[31] L. C. Gilday, S. W. Robinson, T. A. Barendt, M. J. Langton, B. R. Mullaney, P. D. Beer, *Chem. Rev.* **2015**, *115*, 7118.
[32] G. Berger, P. Frangville, F. Meyer, *Chem. Commun.* **2020**, *56*, 4970.
[33] P. Politzer, J. S. Murray, T. Clark, *Phys. Chem. Chem. Phys.* **2013**, *15*, 11178.
[34] G. R. Desiraju, P. S. Ho, L. Kloo, A. C. Legon, R. Marquardt, P. Metrangolo, P. Politzer, G. Resnati, K. Rissanen, *Pure Appl. Chem.* **2013**, *85*, 1711.
[35] T. H. Borchers, F. Topić, J. C. Christopherson, O. S. Bushuyev, J. Vainauskas, H. M. Titi, T. Friščić, C. J. Barrett, *Nat. Chem.* **2022**, *14*, 574.
[36] J. Y. C. Lim, P. D. Beer, *Chem* **2018**, *4*, 731.
[37] A. Mukherjee, S. Tothadi, G. R. Desiraju, *Acc. Chem. Res.* **2014**, *47*, 2514.

[38] R. Kampes, S. Zechel, M. D. Hager, U. S. Schubert, *Chem. Sci.* **2021**, *12*, 9275.
[39] L. Canil, J. Salunke, Q. Wang, M. Liu, H. Köbler, M. Flatken, L. Gregori, D. Meggiolaro, D. Ricciarelli, F. De Angelis, M. Stolterfoht, D. Neher, A. Priimagi, P. Vivo, A. Abate, *Adv. Energy Mater.* **2021**, *11*, 2101553.
[40] A. Abate, M. Saliba, D. J. Hollman, S. D. Stranks, K. Wojciechowski, R. Avolio, G. Grancini, A. Petrozza, H. J. Snaith, *Nano Lett.* **2014**, *14*, 3247.
[41] W. Dai, X. Niu, X. Wu, Y. Ren, Y. Zhang, G. Li, H. Su, Y. Lei, J. Xiao, J. Shi, B. Tong, Z. Cai, Y. Dong, *Angew. Chem. Int. Ed.* **2022**, *61*, e202200236.
[42] Z.-Y. Zhang, Y. Chen, Y. Liu, *Angew. Chem. Int. Ed.* **2019**, *58*, 6028.
[43] A. Abe, K. Goushi, M. Mamada, C. Adachi, *Adv. Mater.* **2023**, https://doi.org/10.1002/adma.202211160.
[44] R. Tepper, S. Bode, R. Geitner, M. Jäger, H. Görls, J. Vitz, B. Dietzek, M. Schmitt, J. Popp, M. D. Hager, U. S. Schubert, *Angew. Chem. Int. Ed.* **2017**, *56*, 4047.
[45] H. Guo, R. Puttreddy, T. Salminen, A. Lends, K. Jaudzems, H. Zeng, A. Priimagi, *Nat. Commun.* **2022**, *13*, 7436.
[46] T. H. Ware, M. E. McConney, J. J. Wie, V. P. Tondiglia, T. J. White, *Science* **2015**, *347*, 982.
[47] H.-H. Yoon, D.-Y. Kim, K.-U. Jeong, S.-k. Ahn, *Macromolecules* **2018**, *51*, 1141.
[48] Q. Zhang, Y. Deng, C.-Y. Shi, B. L. Feringa, H. Tian, D.-H. Qu, *Matter* **2021**, *4*, 1352.
[49] H. Guo, Y. Han, W. Zhao, J. Yang, L. Zhang, *Nat. Commun.* **2020**, *11*, 2037.
[50] S.-M. Kim, H. Jeon, S.-H. Shin, S.-A. Park, J. Jegal, S. Y. Hwang, D. X. Oh, J. Park, *Adv. Mater.* **2018**, *30*, 1705145.
[51] K. E. Riley, J. S. Murray, J. Fanfrlík, J. Řezáč, R. J. Solá, M. C. Concha, F. M. Ramos, P. Politzer, *J. Mol. Model.* **2011**, *17*, 3309.
[52] M. Saccone, V. Dichiarante, A. Forni, A. Goulet-Hanssens, G. Cavallo, J. Vapaavuori, G. Terraneo, C. J. Barrett, G. Resnati, P. Metrangolo, A. Priimagi, *J. Mater. Chem. C* **2015**, *3*, 759.
[53] W. Zou, J. Dong, Y. Luo, Q. Zhao, T. Xie, *Adv. Mater.* **2017**, *29*, 1606100.
[54] T. Clark, M. Hennemann, J. S. Murray, P. Politzer, *J. Mol. Model.* **2007**, *13*, 291.
[55] P. Metrangolo, J. S. Murray, T. Pilati, P. Politzer, G. Resnati, G. Terraneo, *CrystEngComm* **2011**, *13*, 6593.
[56] T. A. Bramlett, A. J. Matzger, *Chem. Eur. J.* **2021**, *27*, 15472.
[57] P. J. Costa, *Phys. Sci. Rev.* **2017**, *2*, 20170136.
[58] S. J. D. Lugger, D. J. Mulder, A. P. H. J. Schenning, *Angew. Chem. Int. Ed.* **2022**, *61*, e202115166.
[59] B. H. Stuart, *Infrared spectroscopy: fundamentals and applications*, John Wiley & Sons, New York, **2004**.
[60] M. T. Messina, P. Metrangolo, W. Navarrini, S. Radice, G. Resnati, G. Zerbi, *J. Mol. Struct.* **2000**, *524*, 87.
[61] Z. Liu, H. K. Bisoyi, Y. Huang, M. Wang, H. Yang, Q. Li, *Angew. Chem. Int. Ed.* **2022**, *61*, e202115755.
[62] Y. Zhang, Z. Wang, Y. Yang, Q. Chen, X. Qian, Y. Wu, H. Liang, Y. Xu, Y. Wei, Y. Ji, *Sci. Adv.* **2020**, *6*, eaay8606.
[63] J.-H. Lee, J. Bae, J. H. Hwang, M.-Y. Choi, Y. S. Kim, S. Park, J.-H. Na, D.-G. Kim, S.-k. Ahn, *Adv. Funct. Mater.* **2022**, *32*, 2110360.
[64] Y. Yao, E. He, H. Xu, Y. Liu, Z. Yang, Y. Wei, Y. Ji, *Nat. Commun.* **2023**, *14*, 3518.
[65] A. Baumann, A. Sánchez-Ferrer, L. Jacomine, P. Martinoty, V. Le Houerou, F. Ziebert, I. M. Kulić, *Nat. Mater.* **2018**, *17*, 523.
[66] S. J. D. Lugger, S. J. A. Houben, Y. Foelen, M. G. Debije, A. P. H. J. Schenning, D. J. Mulder, *Chem. Rev.* **2022**, *122*, 4946.

Manuscript received: July 3, 2023
Accepted manuscript online: September 11, 2023
Version of record online: September 19, 2023